

Detection of OH Towards the Extreme Carbon Star IRC+10216

K. E. Saavik Ford, David A. Neufeld

*Dept. of Physics & Astronomy, The Johns Hopkins University, 3400 N. Charles St.,
Baltimore, MD 21218-2686*

saavik@pha.jhu.edu, neufeld@pha.jhu.edu

Paul F. Goldsmith,

*National Astronomy and Ionosphere Center, Department of Astronomy, Cornell
University, 610 Space Sciences Building, Ithaca, NY 14853-6801*

pfg@astrosun.tn.cornell.edu

and

Gary J. Melnick

Harvard-Smithsonian Center for Astrophysics, 60 Garden Street, Cambridge, MA 02138

melnick@cfa.harvard.edu

ABSTRACT

We report the detection of the 1665 and 1667 MHz main lines of OH (hydroxyl) and upper limits on the 1612 MHz satellite line of OH towards the carbon-rich AGB star, IRC+10216. We find a beam averaged fractional abundance $x(\text{OH}) \sim 4 \times 10^{-8}$. This detection supports the identification by Melnick et al. (2001) of the $1_{10} - 1_{01}$ transition of water vapor with a 556.936 GHz emission feature detected towards IRC+10216, since OH is the expected photodissociation product of water vapor. The shape of the OH lines, however, differs significantly from the shape expected based on the observations of Melnick et al. (2001). Possible explanations for the anomalous shapes of the 1665 and 1667 MHz lines are discussed. The most likely explanations for the unexpected OH line shapes are either masing or an asymmetric distribution of OH molecules around IRC+10216.

Subject headings: Kuiper Belt – planetary systems – comets: general – stars: AGB and post-AGB – stars: individual (IRC+10216) – radio lines: stars

1. Introduction

IRC+10216 is the prototypical late-stage, carbon-rich asymptotic giant branch (AGB) star. This star is extremely well-studied, due to its close proximity and large mass loss rate; the star is losing mass at a rate of $\sim 3 \times 10^{-5} M_{\odot} \text{ yr}^{-1}$ (Glassgold 1996), producing a dense, dusty circumstellar envelope, well shielded from interstellar ultraviolet (ISUV) radiation. The dense, shielded environment of IRC+10216’s envelope is home to a rich circumstellar chemistry. To date, more than 50 molecules have been detected around IRC+10216. Due to the extreme carbon-rich nature of the source ($C/O \gtrsim 1.4$) (Glassgold 1996), the detection of any oxygen-bearing molecules other than CO and small amounts of SiO and HCO^+ was entirely unexpected. Recently, however, Melnick et al. (2001) reported the detection of an emission feature at 556.936 GHz, attributed to the $1_{10} - 1_{01}$ transition of water vapor. The detection of water vapor in such a carbon-rich circumstellar envelope was interpreted by Melnick et al. (2001) as evidence for the existence of an extrasolar cometary system, analogous to the Solar System’s Kuiper Belt, in orbit around IRC+10216. In this system, the luminosity of the central star has increased dramatically due to the later stages of post-main sequence stellar evolution, causing the icy bodies in the Kuiper Belt analog to vaporize (Ford & Neufeld 2001) and produce the water vapor observed by Melnick et al. (2001).

Of possible concern for the cometary hypothesis is the existence of a peculiar subclass of carbon stars which exhibit OH and H_2O maser emission, as well as silicate emission features (e.g. Engels 1994). These features would normally be unexpected in carbon stars, for the reasons explained above. This subclass also shows a number of other features which distinguish peculiar carbon stars from normal carbon stars, including relatively high $^{13}\text{C}/^{12}\text{C}$ ratios, IRAS colors compatible with low mass loss rate oxygen stars, and depleted s-process element abundances relative to other carbon stars. These peculiar carbon stars may represent objects in the transition stage between oxygen star and carbon star, and their photospheric chemistry is likely to be out of thermochemical equilibrium, or they may be members of binary pairs of one oxygen star and one carbon star (Wallerstein & Knapp 1998). In any case, IRC+10216 displays none of the ancillary characteristics associated with these peculiar carbon stars, aside from OH and H_2O emission. Due to the large C/O ratio in IRC+10216 and the fact that it is not a member of a binary system, as well as the lack of ancillary characteristics, we exclude the possibility that OH or H_2O emission from IRC+10216 arises from membership in this peculiar class of carbon stars.

Since the Melnick et al. (2001) result was based on the detection of a single line of water vapor, we became interested in finding a method of verifying the identification of water vapor with the emission feature at 556.936 GHz. To this end, we realized that the water vapor emitted by icy bodies in the cometary system would be carried by the circumstellar outflow

and shielded by the dust, until the outflow became diffuse enough to allow penetration by the ISUV field. Once the ISUV field could penetrate the outflow, the water vapor would be photodissociated into OH and atomic hydrogen. The OH could be detected, and such a detection would yield support for the Melnick et al. (2001) identification. Based on our model for the production of OH, we proposed a deep search for OH around IRC+10216 (a previous search by Andersson, Wannier & Lewis (1992) resulted in a non-detection); we were awarded 30 nights at the Arecibo Observatory¹ for our search. We present our observations in §2, discuss the implications of our results in §3 and present our conclusions in §4.

2. Observations

The radio telescope at Arecibo Observatory (AO) is an altitude-azimuth telescope with a fixed 304.8 m primary spherical reflector and a movable Gregorian dome which contains secondary and tertiary reflectors, as well as multiple receivers. For the observations discussed in this paper, the L-wide receiver was used with dual linear polarizations with each of four boards of the correlator in a 9-level mode, centered on the frequency of interest and covering a bandwidth of 3.125 MHz divided into 1024 channels, resulting in an unsmoothed velocity resolution of 0.55 km s^{-1} at 1665 and 1667 MHz. Observations were taken 2001 November 27 – December 10; 2002 February 2 – 3, 12, 14, 23; 2002 March 2 – 4, 24, 27 – 31; and 2002 April 1, which resulted in a total on-source integration time of 1613 minutes. At least one flux calibration was done during each observing session, on one, two or three of the following sources: B0838+133, J0935+086, B1117+146, B1040+123 or B1005+077, depending upon the amount of time available. Our calibration sources were observed at a variety of zenith angles, so we may take an average gain from these measurements as representative of the telescope gain for our target observations. We found the telescope gain to be 8.2 K/Jy at 1666 MHz. All observations were conducted using standard position switching, with equal duration 5 minute on-source and off-source scans, except on 2001 November 28, when the scan duration varied between 3 and 5 minutes in an effort to maximize observing time. The transitions of primary interest, the 1665 and 1667 MHz main lines of OH, were observed during all sessions. Other transitions which were only observed during some of the sessions were the 1612 and 1721 MHz satellite lines of OH, the 1420 MHz hyperfine line of HI, the 1347 MHz $2_{-1} - 2_1$ line of $\nu_2 = 1$ HCN and the 1743 MHz $3 - 2$ line of HC_9N .

Data reduction was accomplished by converting the raw AO data to Continuum and Line

¹The Arecibo Observatory is part of the National Astronomy and Ionosphere Center, which is operated by Cornell University under a cooperative agreement with the National Science Foundation.

Analysis Single-dish Software (CLASS) format. To prevent contamination of the data by RFI signals, each scan was examined by eye, and any scans with apparent RFI (i.e. those with prominent, rapidly varying signals) were eliminated. The remaining scans were summed to produce a total spectrum for each observed frequency. The total spectrum was then smoothed, using the CLASS “smooth” macro, resulting in a smoothed velocity resolution of 1.1 km s^{-1} . A first order polynomial baseline was subtracted from the smoothed data. In the case of the OH main lines, an emission feature was readily apparent in the final data, and a Gaussian profile was fit to each feature. The calibrated main line spectra, together with the Gaussian fits, are displayed in Figure 1. The fit parameters for these lines are listed in Table 1. The errors listed in the table are 1σ ; thus the 1665 and 1667 MHz lines are detected at a significance of 4.7σ and 8.8σ , respectively. We determine an average fractional abundance for OH of $x(\text{OH}) \sim 4 \times 10^{-8}$ using the 1667 MHz line flux, $F_{1667} = 39 \text{ mK km s}^{-1} = 4.8 \text{ mJy km s}^{-1}$, and the relationship between F_{1667} and the number of OH molecules, $N(\text{OH}) = 4\pi D^2 F_{1667} / f_u A_{ul} h\nu$, where $D = 170 \text{ pc}$ is the distance to IRC+10216, $f_u = 5/16$ is the fraction of molecules in the upper state (the value of $5/16$ is plausible for the most likely excitation conditions), $A_{ul} = 7.8 \times 10^{-11} \text{ s}^{-1}$ is the Einstein A coefficient for the transition and $h\nu$ is the energy of the transition. Once we have found $N(\text{OH})$, we may divide by the number of H nuclei in the Arecibo beam to find $x(\text{OH})$. Based on a density of H nuclei of $n_H = 3 \times 10^{37} (\dot{M}_{-5} / v_{exp,6}) / r^2 \text{ cm}^{-3}$ (Glassgold, 1996), where $\dot{M}_{-5} = 3$ is the stellar mass loss rate in units of $10^{-5} M_\odot \text{ yr}^{-1}$, and $v_{exp,6} = 1.4$ is the expansion velocity² of the circumstellar envelope in units of 10^6 cm s^{-1} , we find 7.8×10^{55} hydrogen nuclei, assuming a maximum radius of $r_{max} = 10^{17} \text{ cm}$. We choose $r_{max} = 10^{17} \text{ cm}$ because we expect nearly all of the OH to lie inside of this radius, and we do not correct for beam sensitivity since this is within the half-power beamwidth of AO and any such correction would be at the level of a few percent at most. This yields a rough determination of $x(\text{OH})$ which is relatively model independent but somewhat misleading. Since we believe the OH to be in a photodissociated shell or ring around IRC+10216, the OH fractional abundance in the outer regions of the circumstellar envelope around IRC+10216 may reach values several times larger than our minimum.

We failed to detect any signal originating in the envelope of IRC+10216 at the five other frequencies we observed. Severe radio frequency interference (RFI) across all observations prevents us from placing meaningful upper limits on the strength of the 1721 MHz satellite line of OH or the 1743 MHz line of HC₉N. Strong contamination from interstellar gas at the

²The expansion velocity determined by Melnick et al. (2001) from the water vapor line in IRC+10216 is $v_{exp,6} = 1.7$. We use $v_{exp,6} = 1.4$ instead, since this is the value found previously for IRC+10216 (e.g. Skinner et al. 1999), and because there are large errors associated with the Melnick et al. measurement.

velocity of IRC+10216 prevents us from making any strong statements about stellar emission at 1420 MHz, the hyperfine line of HI. Our results suggest the necessity of interferometric observations to detect and map the contribution to HI emission from the star. For the remaining lines, we were able to determine upper limits on the observed flux. These are also listed in Table 1.

3. Discussion

In conjunction with the observations discussed above, we constructed several models which attempted to predict the strength and shape of the OH lines in IRC+10216. First, we used a photodissociation model for H₂O and OH, assuming a dusty spherical outflow, illuminated from the exterior by the interstellar ultraviolet (ISUV) field. We used photodissociation rates and dust opacities based on Roberge et al. (1991). The rates in Roberge et al. (1991) were calculated for a plane-parallel slab, so a correction for the spherical geometry of the circumstellar envelope around IRC+10216 was applied. This correction is described in detail in Appendix A. Our model assumed spherical shielding of the molecules due to the spherical distribution of dust around IRC+10216, but did not assume a spherical molecular distribution, since molecular self-shielding was neglected, as is appropriate under the condition of small molecular abundances. A given model produces the relative abundance of H₂O and OH as a function of radial distance. We generated a number of abundance distributions by varying the unshielded molecular photodissociation rate, the stellar mass loss rate, \dot{M} , and the dust opacity. The unshielded molecular photodissociation rate yields the strength of the ISUV field, the stellar mass loss rate determines the density of the shielding dust, and the dust opacity indicates the shielding strength of the dust. Photodissociation models were parameterized by assuming a photodissociation rate, Γ_i , of the form $\Gamma_i(A_v) = 2C_i G_0 \exp(-\alpha_i A_v - \beta_i A_v^2) s^{-1}$, where i represents either OH or H₂O, A_v is the depth in visual magnitudes and C_i , α_i and β_i are factors derived from Roberge et al. (1991) using the procedure described in Appendix A. The factor G_0 represents the relative strength of the ISUV field and $G_0 = 1$ defines the average ISUV field (Draine 1978). We also considered variations in the ratio of A_v to N_H , where N_H is the column density of hydrogen nuclei. This ratio, A_v/N_H , represents how much extinction, and therefore molecular shielding, is produced per unit column density of hydrogen nuclei. For standard interstellar grains considered by Roberge et al. (1991), $A_v/N_H = (A_v/N_H)_0 \equiv 5.6 \times 10^{-22} \text{ mag cm}^{-2}$. The photodissociation model was then used as an input to a second program, which calculated the expected strength and shape of the OH emission lines, including instrumental effects (ie: convolution of beam sensitivity with target intensity) and Gaussian microturbulence. For the beam convolution, we assumed the antenna response is a Gaussian, with $\theta_e = 104''$ where

θ_e is the angular scale on which the sensitivity is reduced by a factor e relative to its on-axis value. This corresponds to a half-power beamwidth, $\text{HPBW} = 2.89'$ (Heiles 1999).

We have chosen five representative photodissociation models, with parameters listed in Table 2, labeled by the letters A through E. Model A assumes the usual ISUV field strength, $G_0 = 1$, normal interstellar grains, $A_v/N_H = (A_v/N_H)_0$, and a mass loss rate, $\dot{M} = 3 \times 10^{-5} M_\odot \text{yr}^{-1}$, which is in the middle of the range of mass loss rates measured for IRC+10216. Models B through E demonstrate the effect of departures from the values of Model A. The results of our photodissociation code for Models A through E are plotted in Figure 2. The solid line represents the fractional abundance of H_2O relative to molecular hydrogen, $x(\text{H}_2\text{O})$, while the dashed line is the fractional abundance of OH relative to molecular hydrogen, $x(\text{OH})$, both as a function of astrocentric radius. All models are normalized to a peak fractional water abundance of $x(\text{H}_2\text{O}) = 1.1 \times 10^{-6}$, consistent with the middle of the range of values for $x(\text{H}_2\text{O})$ determined by Melnick et al. (2001) from observations of the water vapor around IRC+10216. Notice that for Models B through D, even relatively large changes (factors of 2 or 3) in the values of G_0 , A_v/N_H and \dot{M} have a relatively small effect on the radial location of the peak in $x(\text{OH})$. The small value of G_0 in Model C and the large value of A_v/N_H in Model D are fairly unrealistic (Jura 1983), but the plots of Models A through D demonstrate the range of possible sizes of the OH shell with even marginally realistic parameters. Indeed, the only photodissociation model which produces a shell significantly larger than Model A is Model E, which requires an implausibly large A_v/N_H and a relatively improbable G_0 .

Initially, we consider the line shape produced by OH distributed in a spherical shell. Based on photodissociation Model A, our line profile program predicted that the OH emission would come from an almost entirely unresolved spherical shell, and the line profile would thus be very nearly a “top hat” profile. The predicted profile is displayed in Figure 3 as line model S1, and the parameters for that line model as well as several other line models are listed in Table 3. After initial observations indicated the absence of detectable emission at -26.5 km s^{-1} , the systemic velocity of the source (Cernicharo, Guélin & Kahane 2000), other models were discussed. One possibility we considered was that the OH shell was larger than we originally predicted, due either to a larger than expected dust opacity or to a weaker than expected ISUV field. If the OH shell were sufficiently enlarged, it would be partially resolved by AO and would produce a double-peaked line profile. Unfortunately, as discussed above, extremely unreasonable parameters are required to produce a substantially enlarged OH shell. Even using photodissociation model C, displayed in Figure 3 as line model S2, the line profile remains essentially a “top hat”. Only photodissociation Model E produces a double peaked line (line model S3 in Figure 3).

The final possibility we considered was an edge-on ring, which would also give rise to a double-peaked profile for the optically thin OH, even if the ring were unresolved. A ring structure for the OH would arise naturally if the water vapor were distributed in a disk, as might be expected for a cometary system analogous to the Kuiper Belt. Several ring profiles are plotted in Figure 4; the input parameters for the ring line models are listed in Table 3 together with the spherical line models. The rings are defined in spherical coordinates as extending from $\theta = \frac{\pi}{2} - \frac{\psi}{2}$ to $\theta = \frac{\pi}{2} + \frac{\psi}{2}$, where ψ is the opening angle of the disk/ring, taken as an adjustable parameter in our model; $\psi = 180$ degrees is a sphere. Note that changing the opening angle from 10 degrees (model R1) to 1 degree (model R2) has little effect on the line shape. We note that an unresolved expanding disk would lead to an elliptical profile for the optically thick water line. The water line profile obtained by Melnick et al. (2001) is plotted in Figure 1. It does not have a sufficiently large signal to noise ratio to distinguish between an elliptical profile and the parabolic profile expected for an expanding sphere. Finally, in model R3, we demonstrate the effect of changing the assumed microturbulent velocity, b , from the value measured previously for several other lines in IRC+10216, $b = 0.65 \text{ km s}^{-1}$ (Skinner et al. 1995), to $b = 2.0 \text{ km s}^{-1}$. Such a change increases the width of the peaks and tends to decrease the ratio of height of the line peak to the height of the line center. The microturbulent velocity of the OH gas could be increased by the injection of energy due to the photodissociation process itself.

Although the predicted line shape varies substantially depending on the parameters of the photodissociation model and geometry, the predicted line strength is primarily a function of the assumed fractional water abundance. For a given photodissociation model and geometry, the line strength varies linearly with assumed fractional water abundance. Unfortunately the fractional water abundance is uncertain by more than a factor of two, with possible values in the range $x(\text{H}_2\text{O}) = 4 - 24 \times 10^{-7}$ and a preferred value of $x(\text{H}_2\text{O}) = 1.1 \times 10^{-6}$ (Melnick et al. 2001). The large range of possible values for the fractional water abundance is due primarily to the uncertainty in the distance to IRC+10216, which is unknown to a factor of ~ 2 . Various authors report reasonable distance estimates between 300 pc (Doty & Leung 1997) and 110 pc (Groenewegen, Van Der Veen & Matthews 1998). We adopt a distance of 170 pc (e.g. Winters, Dominik & Sedlmayr 1994; LeBertre 1997; Skinner et al. 1999) throughout. For line model S1 (based on photodissociation model A) and $x(\text{H}_2\text{O}) = 1.1 \times 10^{-6}$, we predict a line strength of $10.5 \text{ mJy km s}^{-1}$ (or $86.1 \text{ mK km s}^{-1}$) for the 1667 MHz line. However, due to the uncertainty in the fractional water abundance, this corresponds to possible line strengths ranging from 3.82 to $22.9 \text{ mJy km s}^{-1}$ (31.3 to 188 mK km s^{-1}). The predicted line fluxes listed in Table 3 are for the 1667 MHz line and are calculated assuming $x(\text{H}_2\text{O}) = 1.1 \times 10^{-6}$. The 1665 MHz line is $5/9$ the strength of the 1667 MHz line in LTE for optically thin emission.

While the observed strengths of the 1667 and 1665 MHz lines agree well with our line strength predictions, the observed OH line shapes are in very poor agreement with our predictions. The observed line profiles are neither “top hats” nor double-peaked; indeed, they are not even symmetric about $v_{LSR} = -26.5 \text{ km s}^{-1}$, the systemic velocity of IRC+10216. This asymmetry is unique³ - every other molecule observed in the outer envelope of IRC+10216 has a profile which is symmetric about the systemic velocity (e.g. Cernicharo et al. 2000). Rather, the 1667 and 1665 MHz emission features are blueshifted with respect to the systemic velocity, and they have central velocities which differ slightly (see Table 1). Based on the errors quoted in Table 1, we might conclude that the velocities of the two features differ at a statistically significant level. However, we note that the errors are based on fitting a Gaussian profile to a line which is not likely to be a true Gaussian. A more appropriate (and conservative) estimate of the error associated with the line center determination is simply the velocity resolution of our spectrum. For the 1665 and 1667 MHz lines, the size of a resolution element after smoothing is 1.1 km s^{-1} . Given this error estimate, we conclude that the 1665 and 1667 MHz lines may have the same central velocity.

For comparison with our pre-observation models, we plot our “best fit” model over the data for the 1667 MHz line in Figure 5. Our “best fit” is model R3, except that we must assume a fractional water abundance of 2.4×10^{-6} in order to match the line fluxes for velocities between -40 and -30 km s^{-1} . Also, in order to match the velocity of the observed line with the blueshifted peak of the model, we assume a $v_{LSR} = -23.5 \text{ km s}^{-1}$, which represents a redshift of 3 km s^{-1} with respect to prior measurements of the v_{LSR} using other species (e.g. Cernicharo et al. 2000). It is obvious from the plot that the blueshifted peak of the model fits the data reasonably well, but the redshifted peak of the model is entirely missing from the data.

The observed shapes of the 1667 and 1665 MHz OH lines are quite unexpected. There are only three general mechanisms which might create the observed line profiles; these mechanisms are: 1) absorption, 2) masing or 3) an intrinsic asymmetry in the spatial distribution of the OH. In the following sections, we examine each mechanism in detail and discuss its plausibility.

³Observations by Lucas & Cernicharo (1989) and Lucas & Guilloteau (1992) found asymmetric line profiles for HCN in IRC+10216. However, this emission originates in the inner regions of the circumstellar outflow (inside the acceleration zone). The observed asymmetry was attributed to masing.

3.1. Absorption

It seems reasonable to begin with the assumption that the OH emission from IRC+10216 is intrinsically symmetric. If that were the case, then in order to explain the OH line shapes, there must exist some absorbing medium within the circumstellar envelope of IRC+10216 which prevents emission from the far (redshifted) side of the envelope from reaching us, while emission from the near (blueshifted) side escapes and is detected. Since these observations were done at wavelengths which are large, relative to previous observations of this star, there is one source of opacity that could have previously gone undetected - electron free-free absorption. However, this absorption would be accompanied by thermal continuum emission. In order to be an effective absorber of the redshifted half of the OH line, the absorber would need to be optically thick at a radius of $\sim 10^{17}$ cm, where the OH distribution peaks (though the peak radius of the OH distribution varies somewhat depending on the parameters of the photodissociation model, 10^{17} cm is a reasonable value for most models). At such a large radius, the envelope gas temperature is quite cold, about 11 K, and the thermal emission from the absorber would correspond to a blackbody at the same temperature. Unfortunately, our observations are not well suited to determining the continuum brightness at 1665 and 1667 MHz, but Sahai, Claussen, & Masson (1989) have observed the continuum brightness at slightly higher frequencies, specifically at 15 and 20 GHz. The predicted flux densities due to free-free emission at 15 and 20 GHz are 250 and 140 mJy, respectively, for an object which is optically thick at 1665 and 1667 MHz. Sahai et al. (1989) find the flux densities to be only 6 and 1.4 mJy at 15 and 20 GHz, respectively. The absence of strong continuum emission indicates that at these frequencies, the envelope of IRC+10216 cannot be optically thick at radii large compared to that of the AO beam, effectively ruling out the absorption scenario. In addition, the electron density required to make the envelope of IRC+10216 optically thick would be substantially in excess of the densities presently expected based on theoretical models of the envelope chemistry.

3.2. Masing

A second possible explanation for the observed line profiles is maser amplification of the 1667 and 1665 MHz lines. This possibility is attractive, because it is the only one which could potentially be responsible for a velocity difference between the 1667 and 1665 MHz lines. While the modeling of circumstellar maser emission is difficult and a detailed model of possible OH masers around IRC+10216 is beyond the scope of this paper, we can compare our observations to other asymptotic giant branch (AGB) stars with known OH maser emission. However, we should be cautious about drawing strong conclusions based on this comparison,

due to the fact that all stars with confirmed circumstellar OH masers are oxygen-rich stars with much higher fractional OH abundances or carbon-rich stars which have recently made the transition from the oxygen-rich state and also have higher fractional OH abundances than IRC+10216.

There is at least one star which is known to have exhibited OH emission with velocity characteristics similar to IRC+10216, albeit at much larger flux densities. In observations reported by Etoaka et al. (2001), the star R Crt displayed maser emission in the 1667 and 1665 MHz main lines, but not in the 1612 MHz satellite line; this in itself is not particularly unusual among stars which exhibit circumstellar OH masers. More importantly, in observations on 1990 November 17, the 1667 and 1665 MHz emission appeared only at velocities blueshifted with respect to the systemic velocity of R Crt, but with velocities which were offset from each other by $\sim 1 \text{ km s}^{-1}$. Significantly, the ratio of the 1667 to 1665 MHz line strengths was ~ 1.7 during this observation, not far from the ratio of 1.8 expected in thermal equilibrium. As the OH emission from R Crt is known to be maser amplified, this example would seem to argue for at least the possibility of masing in IRC+10216.

Several objections may be raised against the masing scenario, however, which would need to be resolved before masing could be accepted as the source of the line profile asymmetry in IRC+10216. The first objection is that the predicted fluxes for IRC+10216 of the 1667 and 1665 MHz lines in LTE from line model S1 are 1.3 and 0.73 mJy km s⁻¹ respectively, for velocities between -40 and -30 km s^{-1} and an $x(\text{H}_2\text{O}) = 4 \times 10^{-7}$. These predictions are only a factor of ~ 4 less than the observed line strengths, even assuming the minimum possible $x(\text{H}_2\text{O})$, and using line model S1, which predicts the smallest flux density for velocities between -40 and -30 km s^{-1} . The substantial blue/red asymmetry of the line flux requires strong masing. The asymmetry of the 1667 MHz line can be quantified by fitting a Gaussian with fixed parameters to the redshifted side of the line and taking a ratio of the 3σ upper limit on redshifted flux, F_{red} , with the measured flux from the blueshifted side of the line, $F_{blue} = 39.0 \text{ mK km s}^{-1}$. For a Gaussian with a line center fixed at $v_{LSR} = -10.9 \text{ km s}^{-1}$ and a fixed width of 5.8 km s^{-1} , we find a flux of $4.38 \pm 11.4 \text{ mK km s}^{-1}$, 3σ . We chose the center of the red feature so that the blue and red sides of the line would be symmetric about $v_{LSR} = -23.5 \text{ km s}^{-1}$. Thus, we find a 3σ upper limit $F_{red}/F_{blue} \leq 0.4$, or an amplification of the blue side of the line by a factor of at least 2.5, clearly requiring significant amplification. If the OH emission is substantially amplified by maser action, the 1667 and 1665 MHz lines ought to have a brightness temperature comparable to or larger than the temperature of the microwave background ($\sim 3 \text{ K}$, or about $3700 \text{ mJy km s}^{-1}$ between -40 and -30 km s^{-1}). This might lead one to conclude, based on our measurements, that the observed 1667 and 1665 MHz lines are too dim to be strongly maser amplified. Although the OH emission is not that bright, if maser amplification were confined to a small spot, the beam dilution in AO's large field of

view could mean that our observations are still consistent with amplification. Specifically, the maser spot would need to have a diameter smaller than 10 arcsec or 1700 AU at a distance of 170 pc, assuming an intrinsic brightness of 3 K or larger. This is not particularly small, considering that OH maser spots around other evolved stars can have diameters smaller than 25 AU (Chapman, Cohen & Saikia 1991), so the dim lines do not exclude masing.

A far stronger objection stems from theoretical models of circumstellar OH masers by Elitzur (1978). Elitzur found that OH masers in oxygen-rich stars were created by pumping from the far-IR emission of warm dust, and that for the 1667 and 1665 MHz main lines, the maser gain is proportional to the density of OH molecules (below a threshold density). Although Elitzur (1978) did not model OH densities or gas temperatures as low as those expected in IRC+10216, a reasonable extrapolation of his models indicates that $|\tau|$ would be $\ll 1$, where τ is the line center optical depth.

3.3. Intrinsic Asymmetry

The only remaining general class of explanations for the OH line asymmetry is an intrinsic asymmetry in the spatial distribution of the OH around IRC+10216. There are two possible mechanisms for producing such a spatially asymmetric distribution. One mechanism is an asymmetric ISUV field in the vicinity of IRC+10216; this would produce a larger fractional abundance of photodissociation products on one side of the circumstellar envelope relative to the other. Since OH is a photodissociation product, this scenario could produce an asymmetric line profile if the viewing geometry were properly aligned. However, all other molecular photodissociation products would then have the same line profile as OH. This is not observed (e.g. Cernicharo et al. 2000).

The other way to produce an asymmetric distribution of OH would be an asymmetric distribution of its parent molecule, H₂O. The observed water vapor emission is essentially symmetric about the systemic velocity of IRC+10216. However, the H₂O emission and the OH emission do not arise from precisely identical spatial regions (see Figure 2). The time required for a parcel of gas to travel a given radial distance can be found from the simple relationship $R = v_{out}t$, where v_{out} is the terminal velocity of the stellar outflow. Due to the direct relationship between the radial coordinate and time ($R = v_{out}t$), the fact that the OH and H₂O are not spatially coincident means that the present distributions of OH and H₂O were formed at two different epochs, and the OH and H₂O need not have identical geometries at the present time. If the spatial distribution of water were asymmetric a few hundred years ago, but is symmetric now, the OH and H₂O observations could be reconciled with the intrinsic asymmetry scenario.

One possible explanation for a change in the distribution of water vapor over such a relatively short timescale involves the time dependence of the stellar mass loss rate. The circumstellar envelope of IRC+10216 contains multiple dust shells which are the result of episodic mass loss. Detailed images of these shells by Mauron & Huggins (1999, 2000), show that the shells are incomplete - they are arcs rather than rings. Additionally, the dust distribution in the innermost regions of the envelope ($r \lesssim 15''$) is an extremely asymmetric bipolar outflow. The timescale on which these dust shells are produced is of order a few hundred years. A new mass loss study by Fong, Meixner & Shah (2003) demonstrates that mass loss in IRC+10216 has been ongoing for at least 7000 years and that mass loss occurred in a clumpy and asymmetric fashion. Rapid variations in the mass loss rate are also possible; recent high-resolution IR images show dust distribution asymmetries on size scales as small as tens of milliarcseconds and imply mass loss variations on timescales of years (Tuthill et al. 2000; Weigelt et al. 2002; Men'shchikov, Hofmann & Weigelt 2002). Ford & Neufeld (2001) showed that the vaporization of water from icy bodies orbiting IRC+10216 is sensitively dependent on the stellar flux impinging on an icy body. Since the dust distribution is highly asymmetric, the luminosity of the central star will “leak” out in an asymmetric and probably quite patchy pattern, after multiple scatterings and dust absorption and re-emission. Thus, the flux impinging on different icy bodies at the same astrocentric radius will not be necessarily be the same; it will depend on the particular geometry of radiation leakage through the circumstellar dust. Therefore, the water vaporization rate from the surface of a particular icy body (and the distribution of water vapor in the circumstellar outflow) will depend very substantially on the time varying dust distribution in the circumstellar outflow. Note that this scenario is still capable of producing the water line profile observed by Melnick et al. (2001). If the water vapor is more or less off to one side of the star (from a terrestrial observer’s perspective), there will be roughly equal amounts of material coming toward us and moving away from us, still yielding a roughly symmetric profile. Additionally, since the water line is optically thick, it is probable that some clumpiness or patchiness in the water distribution would be smoothed out in the line profile.

4. Summary

We have detected the 1665 and 1667 MHz lines of OH in emission towards the carbon-rich AGB star IRC+10216. This detection supports the identification of the 556.936 GHz emission detected toward IRC+10216 by Melnick et al. (2001) with the $1_{10} - 1_{01}$ transition of water vapor. The 1665 and 1667 MHz line profiles are unexpectedly narrow and blueshifted with respect to the systemic velocity of IRC+10216. We believe that the unanticipated line shape is the result of either maser amplification or some intrinsic spatial asymmetry

in the OH distribution around IRC+10216, or possibly both. While we favor the spatial asymmetry explanation, due to early theoretical work by Elitzur (1978), further modeling of the excitation conditions of OH around IRC+10216 using a code which includes strong masing would help clarify the possible role of maser amplification in this source. Additional theoretical work may also be required to understand the potential spatial asymmetry of OH, despite the apparent symmetry of its parent molecule, H₂O. Finally, while it would be most desirable to spatially resolve the OH emission in IRC+10216, such observations cannot presently be completed within an acceptable amount of telescope time.

We are grateful to the staff at AO, particularly Chris Salter, Phil Perillat, Karen O’Neil and Mike Nolan. We are especially grateful for the outstanding service observing work performed by Hector Hernandez. We would also like to thank Jennifer Wiseman, David Hollenbach, Al Glassgold and Barry McKernan for helpful discussions. This work was supported by subcontract SV252005 from the Smithsonian Institution; K.E.S.F. was also supported by an American Dissertation Fellowship from the American Association of University Women (AAUW). The National Astronomy and Ionosphere Center is operated by Cornell University under a cooperative agreement with the National Science Foundation.

A. Correction to Photodissociation Rates due to Spherical Symmetry

For the purposes of work described in this paper, we want a simple expression for the photodissociation rates of H₂O and OH as a function of depth, measured in magnitudes of visual extinction, A_v , in a sphere which is illuminated isotropically from the exterior by the ISUV field. Calculations done by Roberge et al. (1991) (R91 hereafter) provide rates for a plane-parallel slab geometry. We describe here a method which can be applied to the rates calculated with plane-parallel geometry which will give approximate rates for the spherical case.

R91 calculated photodissociation and photoionization rates for a number of species, as a function of visual extinction into plane-parallel clouds illuminated isotropically from both sides by the average ISUV field (Draine 1978). In general, the photodestruction rate, Γ , for a species, i , is

$$\Gamma_i(A_v) = 4\pi \int_{\lambda_H}^{\lambda_i} J_\lambda(A_v) \sigma_i(\lambda) d\lambda. \quad (\text{A1})$$

The rate, Γ_i , depends on the extinction, A_v , measured inward from the surface of the cloud in units of visual magnitudes. Here $\sigma_i(\lambda)$ is the wavelength dependent cross section for the process of interest, and the integration runs from $\lambda_H = 91.2$ nm to the threshold wavelength

λ_i for the process of interest. The quantity $J_\lambda(A_v)$ is the mean intensity of radiation at depth A_v in photons $\text{cm}^{-2} \text{s}^{-1} \text{sr}^{-1} \text{nm}^{-1}$. R91 used the spherical harmonics method to solve numerically the radiative transfer equation for $J_\lambda(A_v)$ for clouds of $A_v^{tot} = 1, 10$ and 100 mag. The solution for $J_\lambda(A_v)$ allowed R91 to calculate the photodestruction rates for a large number of species at various depths A_v into each of their model clouds ($A_v^{tot} = 1, 10$ and 100 mag). In addition, R91 found that a bi-exponential function, of the form

$$\Gamma_i(A_v) = C_i \exp(-\alpha_i A_v - \beta_i A_v^2) \text{ s}^{-1} \quad (\text{A2})$$

provided a reasonable fit to their numerical results, where C_i is the unattenuated photodestruction rate and α_i and β_i are fit parameters, for a given species i .

A point P in the interior of an R91 plane-parallel slab is illuminated by radiation coming from many directions. If we consider a slab with $A_v = 100$, we can assume that near one surface of the slab, essentially all photodissociating radiation originates at the nearer surface. Under such conditions, the point P “sees” rays diminished by an “effective visual extinction”, $A'_v = A_v / \cos \theta$ coming from a direction θ , where the angle is measured from the normal to the slab and A_v is the depth measured from the surface of the cloud to the point P along the normal ray. In order to calculate photodissociation rates valid for a point Q interior to a sphere, we realized that we should decompose the photodissociating radiation arriving at point P inside a slab into constituent rays coming from a direction θ . This would give us the photodissociation rate due to a single ray. Then, we can use the result for a single ray to integrate over all rays arriving at the point Q in the interior of the sphere. Such a point Q “sees” rays diminished by a different “effective visual extinction”, $A''_v = \theta A_v / \sin \theta$. We can then integrate over all rays arriving at point Q , to determine the total photodissociation rate for a point internal to a sphere.

So, given a formula for the photodissociation rate $\Gamma_i^{pp} = C_i \exp(-\alpha_i^{pp} A_v - \beta_i^{pp} A_v^2)$ in a plane-parallel slab, we should be able to find best fit values for the parameters α_i^r and β_i^r subject to the condition that

$$\frac{|\Gamma_i^{pp} - \Gamma_i^{pr}|}{\Gamma_i^{pp}} \leq 0.2 \quad (\text{A3})$$

for all A_v of interest, where

$$\Gamma_i^{pr} = C_i \int_0^{\pi/2} \exp\left(-\alpha_i^r A'_v - \beta_i^r (A'_v)^2\right) \sin \theta d\theta. \quad (\text{A4})$$

Here Γ_i^{pr} is the best fit photodissociation rate at a point P interior to a plane-parallel slab, found by integrating over each individual ray terminating at point P . The parameters α_i^r and β_i^r are simply the attenuation parameters along any single ray. Once we have α_i^r and

β_i^r , we can repeat a similar procedure to find a best fit α_i^{sp} and β_i^{sp} . Specifically, we wish to satisfy the condition

$$\frac{|\Gamma_i^{sr} - \Gamma_i^{sp}|}{\Gamma_i^{sr}} \leq 0.2 \quad (\text{A5})$$

for all A_v of interest, where

$$\Gamma_i^{sr} = C_i \int_0^\pi \exp\left(-\alpha_i^r A_v'' - \beta_i^r (A_v'')^2\right) \sin \theta d\theta \quad (\text{A6})$$

and

$$\Gamma_i^{sp} = 2C_i \exp(-\alpha_i^{sp} A_v - \beta_i^{sp} A_v^2). \quad (\text{A7})$$

Here Γ_i^{sr} is the photodissociation rate at a point Q interior to a sphere, which is found by integrating over all single rays arriving at point Q (calculated using α_i^r and β_i^r which were found previously to fit the attenuation along a single ray). Γ_i^{sp} is a simple, though approximate, expression for the photodissociation rate at a point Q interior to a sphere, and α_i^{sp} and β_i^{sp} are the best fit attenuation parameters for points interior to a sphere.

In the particular situation of a circumstellar envelope, we note that most of the photodissociation of H_2O and OH occurs at low A_v , near the surface of the sphere, and thus it is most important that Γ_i^{sp} be accurate for relatively small A_v . To that end, we fit our own bi-exponential to the tabulated photodissociation rates at small A_v from R91, which yielded the α_i^{pp} and β_i^{pp} , listed in Table 4. We then applied the fitting procedure described above and found values for α_i^r , β_i^r , α_i^{sp} and β_i^{sp} , also listed in Table 4.

REFERENCES

- Andersson, B.-G., Wannier, P.G., & Lewis, B.M. 1992, MNRAS, 254, 7
- Cernicharo, J., Guélin, M., & Kahane, C. 2000, A&AS, 142, 181
- Chapman, J. M., Cohen, R. J., & Saikia, D. J. 1991, MNRAS, 229, 247
- Doty, S. D., & Leung, C. M. 1997, MNRAS, 286, 1003
- Draine, B. T. 1978, ApJS, 36, 595
- Elitzur, M. 1978, A&A, 62, 305
- Engels, D. 1994, A&A, 285, 497
- Etoka, S., Blaszkiewicz, L., Szymczak, M., & Le Squeren, A.M. 2001, A&A, 378, 522
- Fong, D., Meixner, M., & Shah, R. Y. 2003, ApJ, 582, L39
- Ford, K.E.S., & Neufeld, D.A. 2001, ApJ, 557, L113

- Groenewegen, M. A. T., Van Der Veen, W. E. C. J., & Matthews, H. E. 1998, *A&A*, 338, 491
- Glassgold, A. E. 1996, *ARA&A*, 34, 241
- Heiles, C. 1999, *Arecibo Technical and Operations Memo 1999-02*
- Jura, M. 1983, *ApJ*, 267, 647
- LeBertre, T. 1997, *A&A*, 324, 1059
- Lucas, R., & Cernicharo, J. 1989, *A&A*, 218, L20
- Lucas, R., & Guilloteau, S. 1992, *A&A*, 259, L23
- Mauron, N., & Huggins, P. J. 1999, *A&A*, 349, 203
- Mauron, N., & Huggins, P. J. 2000, *A&A*, 359, 707
- Melnick, G. J., Neufeld, D. A., Ford, K. E. S., Hollenbach, D. J., & Ashby, M. L. N. 2001, *Nature*, 412, 160
- Men'shchikov, A. B., Hofmann, K.-H., & Weigelt, G. 2002, *A&A*, 392, 921
- Roberge, W.G., Jones, D., Lepp, S., & Dalgarno, A. 1991, *ApJS*, 77, 287
- Sahai, R., Claussen, M. J., & Masson, C. R. 1989, *A&A*, 220, 92
- Skinner, C. J., Justtanont, K., Tielens, A. G. G. M., Betz, A. L., & Boreiko, R. T. 1995, *ASP Conf. Ser. 73, Airborne Astronomy Symp. on the Galactic Ecosystem: From Gas to Stars to Dust*, ed. M. R. Haas, J. A. Davidson, & E. F. Erickson (San Francisco: ASP), 433
- Skinner, C. J., Justtanont, K., Tielens, A. G. G. M., Betz, A. L., Boreiko, R. T., & Baas, F. 1999, *MNRAS*, 302, 293
- Tuthill, P. G., Monnier, J. D., Danchi, W. C., & Lopez, B. 2000, *ApJ*, 543, 284
- Wallerstein, G., & Knapp, G. R. 1998, *ARA&A*, 36, 369
- Weigelt, G., Balega, Y. Y., Blöcker, T., Hofmann, K.-H., Men'shchikov, A. B., & Winters, J. M. 2002, *A&A*, 392, 131
- Winters, J. M., Dominik, C., & Sedlmayr, E. 1994, *A&A*, 288, 255

Table 1. Line Fit Parameters And Upper Limits

Species	Frequency (MHz)	Line Strength (mK km s ⁻¹)	Line Center (v_{LSR} in km s ⁻¹)	Line Width (FWHM in km s ⁻¹)
H ₂ O ^a	556936	414 ± 17	-24.7 ± 0.2	24.2 ± 0.2
OH	1667	39.0 ± 4.45	-36.1 ± 0.34	5.8 ± 0.71
OH	1665	23.7 ± 5.05	-38.7 ± 0.58	5.8 ± 1.52
OH	1612	<22.6 (3 σ) ^b		
HCN	1347	<48.9 (3 σ) ^c		

Note. — We list the line fit parameters for spectra displayed in Figure 1, as well as the upper limits on other observed frequencies where no lines were detected.

^aThese values correct a small error in the fit to the SWAS spectrum reported by Melnick et al. (2001). The dashed line in Figure 1 is a plot of the corrected fit. The fitted values assume a parabolic line shape, and the quoted errors are formal errors derived from a 3 parameter fit. Due to the uncertainty in the intrinsic line shape, a more appropriate estimate of the velocity errors is simply the size of a velocity resolution element, 1.1 km s⁻¹. The v_{LSR} of IRC+10216 measured by the water vapor data is therefore consistent with previous measurements of the v_{LSR} of the source.

^bAssumes a line width of 5.8 km s⁻¹.

^cAssumes a line width of 30 km s⁻¹.

Table 2. Photodissociation Models

Model	\dot{M} $10^{-5}(\text{M}_{\odot} \text{yr}^{-1})$	G_0	$\frac{A_v/N_H}{(A_v/N_H)_0}$
A	3	1	1
B	5	1	1
C	3	1/3	1
D	3	1	2
E	3	1/3	9

Table 3. Line Profile Models

Model	Photodissociation Model	Opening angle, ψ (degrees)	b (km s ⁻¹)	Flux (mJy km s ⁻¹)
S1	A	180	0.65	10.5
S2	C	180	0.65	18.1
S3	E	180	0.65	23.9
R1	A	10	0.65	10.6
R2	A	1	0.65	10.6
R3	A	0.1	2.0	10.6

Table 4. α_i and β_i Coefficients for H₂O and OH.

Species	C (s ⁻¹)	α^{pp}	β^{pp}	α^r	β^r	α^{sp}	β^{sp}
H ₂ O	3.19×10^{-10}	3.03	-0.180	1.73	0.00	2.22	0.00
OH	1.90×10^{-10}	3.13	-0.195	1.77	0.00	2.26	0.00

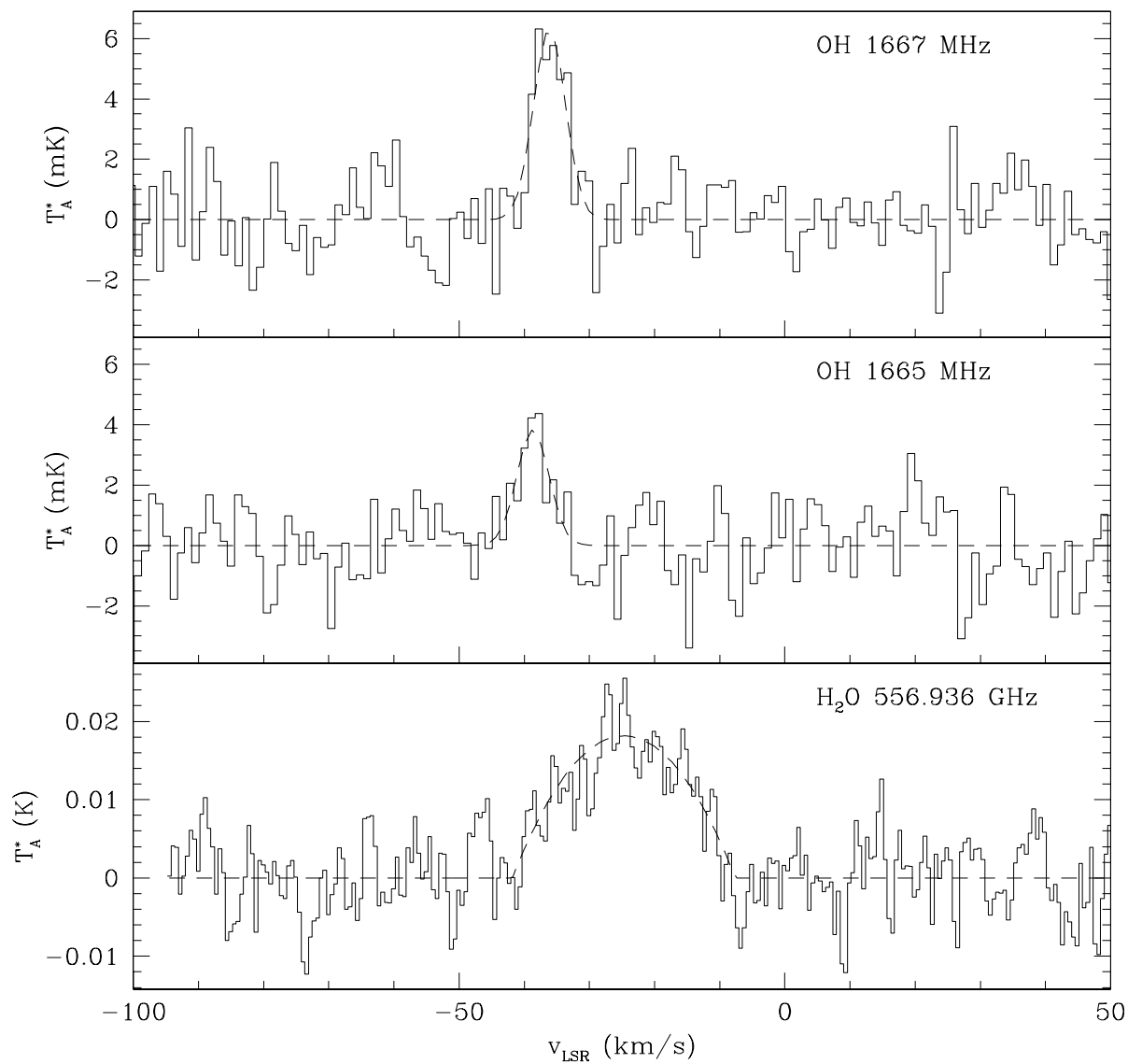


Fig. 1.— Spectra of IRC+10216 at 556.936 GHz (Melnick et al. 2001), and 1665 and 1667 MHz. For the 556.936 GHz line, the dashed line is a fitted parabola, as expected for an optically thick expanding spherical shell. The dashed lines in the 1665 and 1667 MHz spectra are fitted Gaussians. Parameters for all fits are listed in Table 1.

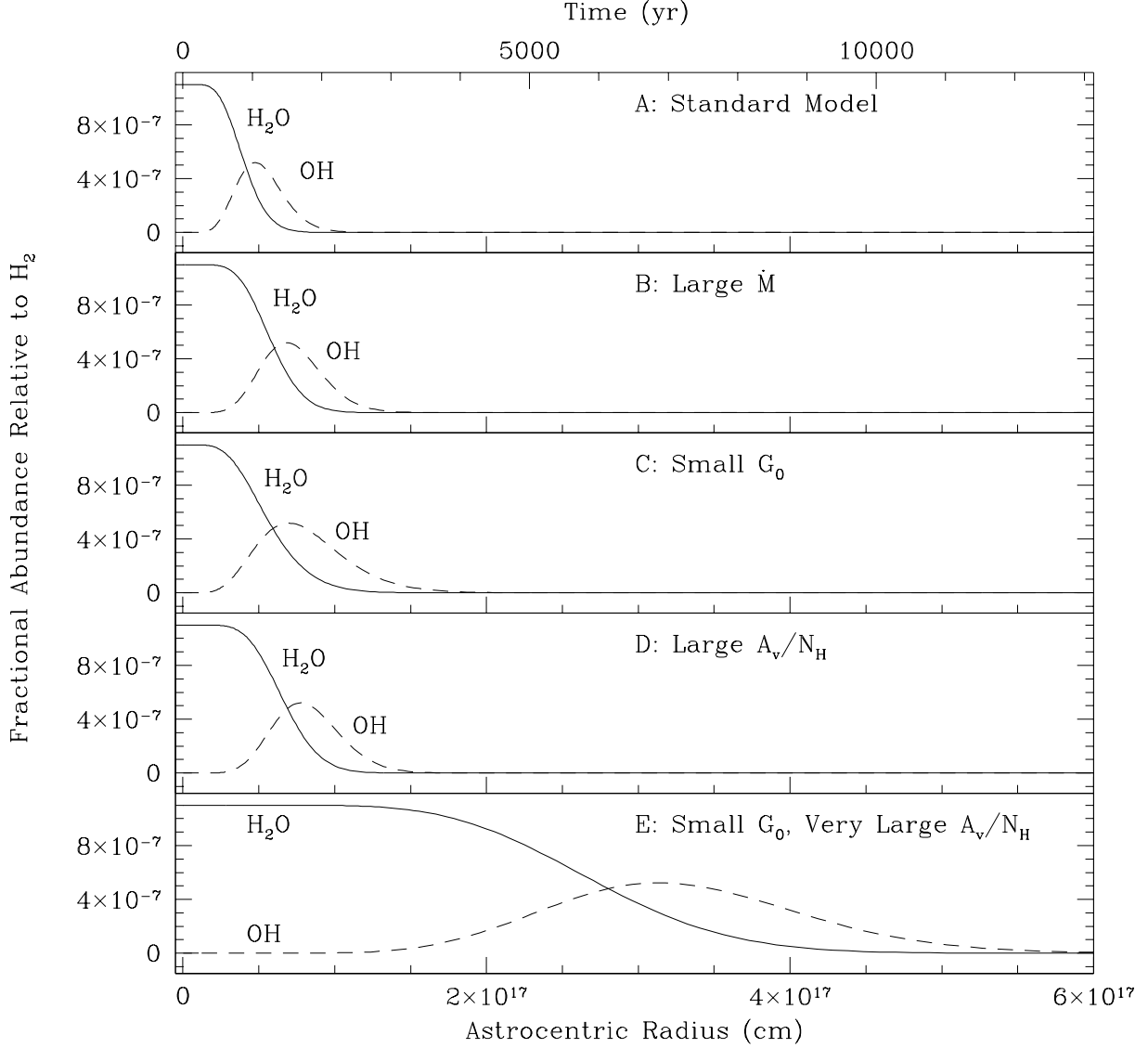


Fig. 2.— Fractional water and OH abundance as a function of radial distance. Also plotted on the upper axis is the time for a parcel of gas to travel a radial distance $R = v_{out}t$, based on a terminal velocity for the circumstellar outflow of $v_{out} = 14.5 \text{ km s}^{-1}$. The solid line is the fractional water abundance and the dashed line is the fractional OH abundance. The fractional abundances are based on the photodissociation models discussed in the text. For input parameters, see Table 2.

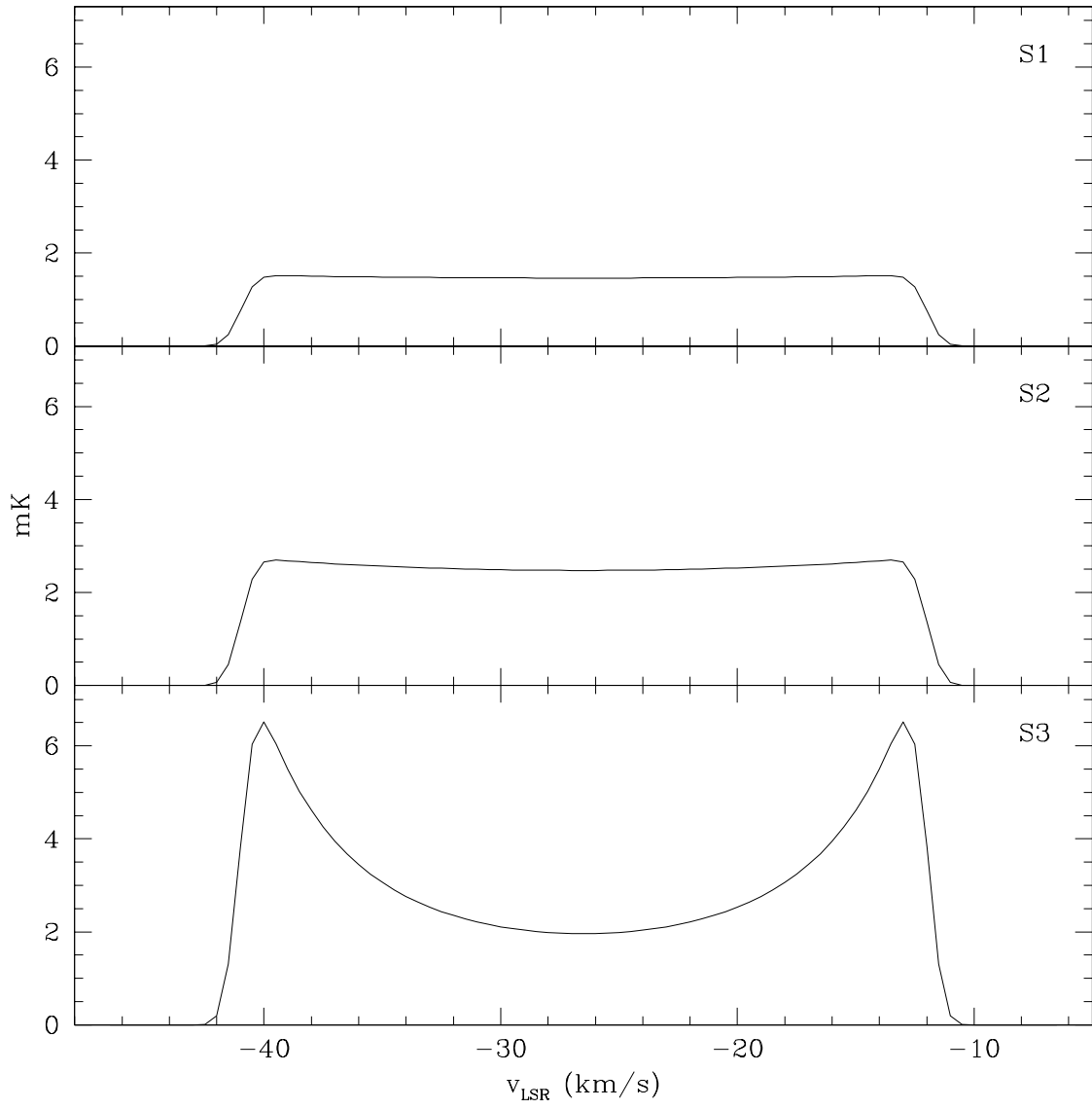


Fig. 3.— Models of line profiles for spherical shells. See Table 3 for input parameters.

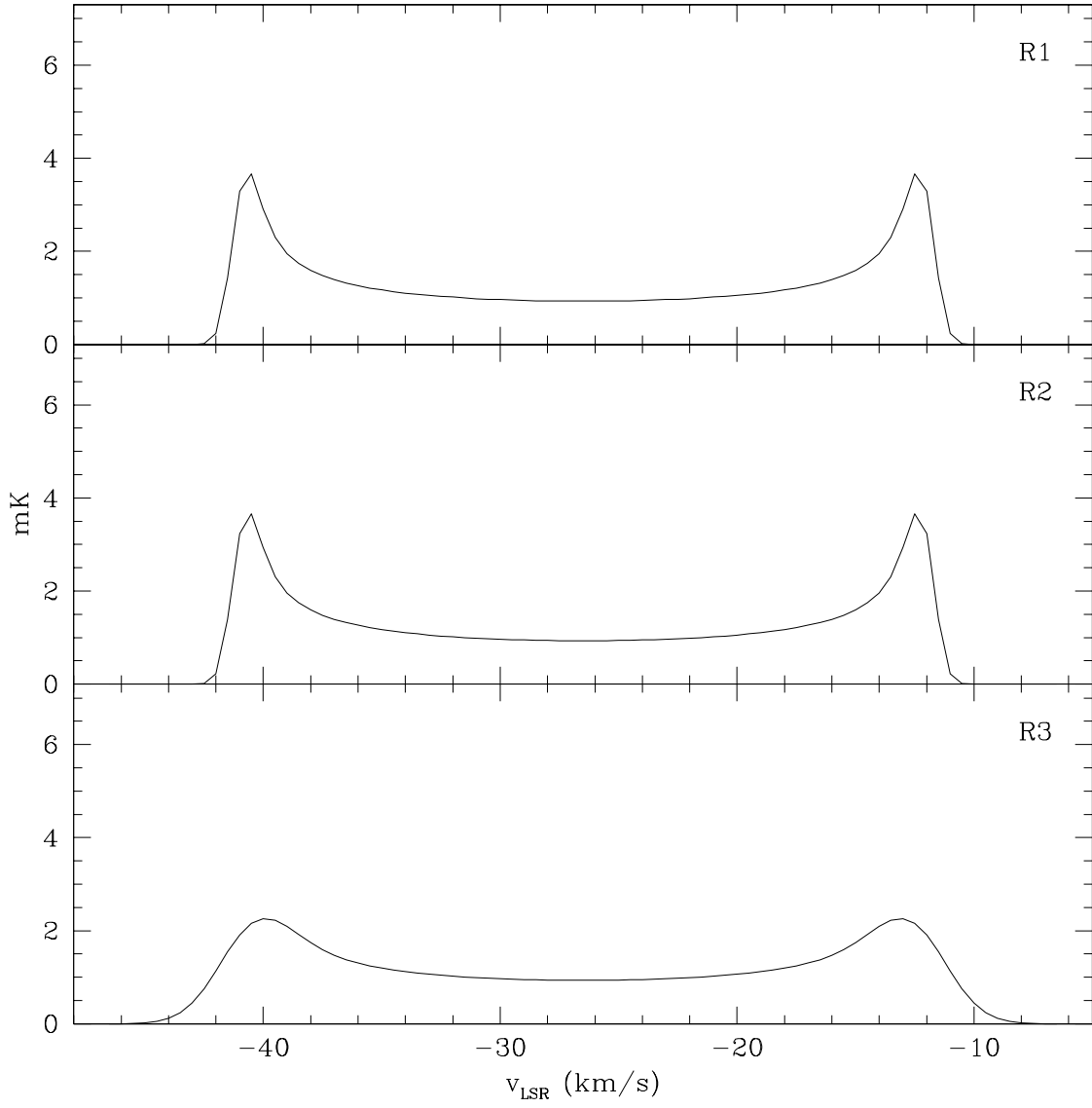


Fig. 4.— Models of line profiles for rings. See Table 3 for input parameters.

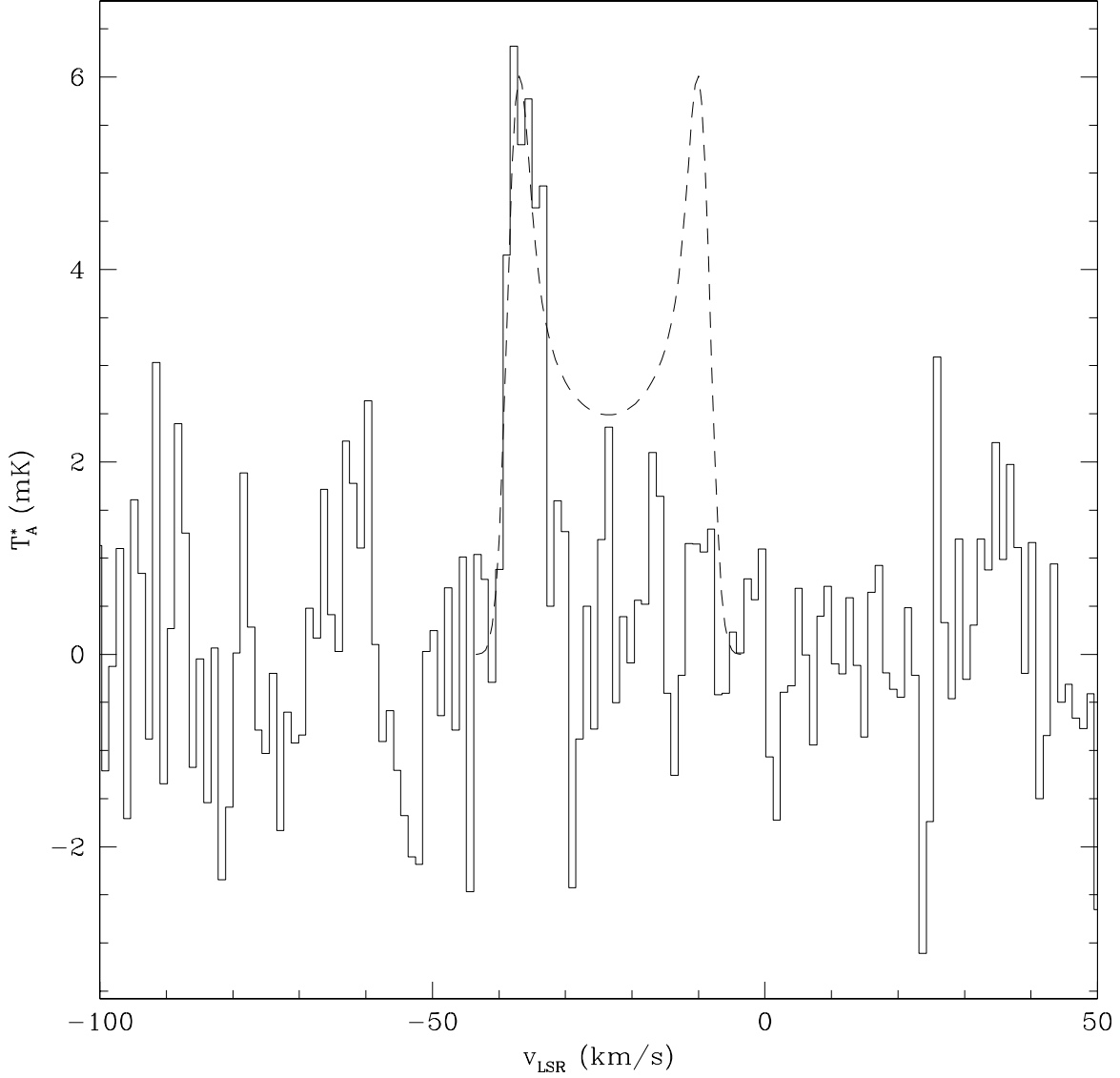


Fig. 5.— 1667 spectrum with best fit model overplotted. Model R3 (see Table 1) provides the best single peak fit. In order to match the velocity of the observed line with the blueshifted peak of the model, we assume a $v_{LSR} = -23.5 \text{ km s}^{-1}$, which represents a redshift of 3 km s^{-1} with respect to prior measurements of the v_{LSR} of IRC+10216 (e.g. Cernicharo et al. 2000). The missing redshifted peak may be explained by a spatially asymmetric distribution of OH or maser amplification of the blueshifted peak (see text for details).